iScience, Volume *23*

Supplemental Information

Distinct Relations of Microtubules and Actin Filaments with Dendritic Architecture

Sumit Nanda, Shatabdi Bhattacharjee, Daniel N. Cox, and Giorgio A. Ascoli

Supplemental Information:

Link to data and code (Mendeley.Com):
DOI: http://dx.doi.org/10.17632/v3ncxmj6fn.1

Supplemental Figures

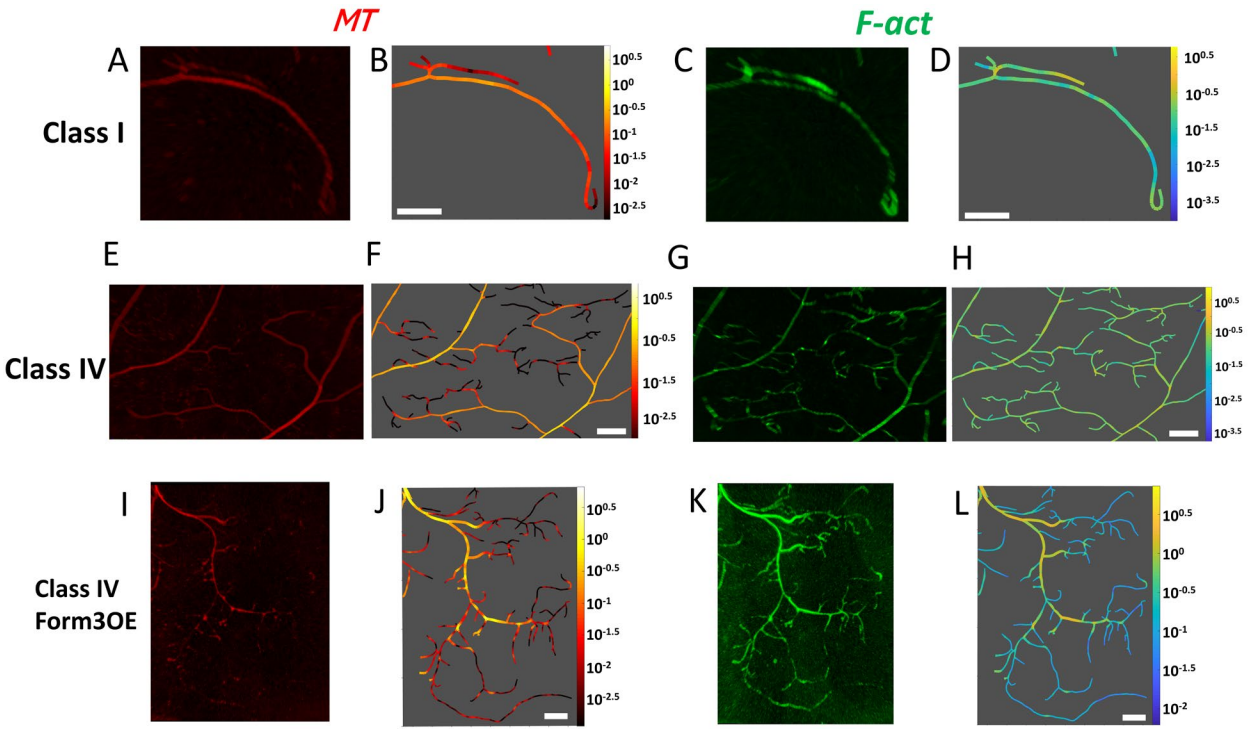

Figure S1. **Image-stacks and multi-signal reconstructions of da neurons. Magnified version of the demarcated regions from Figure 1.** Confocal images and multi-signal reconstructions of Class I wild type (A, B, C, D), Class IV wild type (E, F, G, H) and Class IV mutant Form3OE (I, J, K, L). Microtubule (A, E, I) and F-actin (C, G, K) signals from confocal image stacks are traced together to produce multi-signal reconstructions, allowing the arbor-wide quantification and graphic rendering of microtubule (B, F, J) and F-actin (D, H, L) quantity (calculated by multiplying the signal intensity of the compartment with the compartment thickness, see Transparent Methods section for details). Here we observe three terminal regions from Class I, Class IV and Class IV Form3OE neurons. White scale bars (B, D, F, H, J, L): 20 μm.

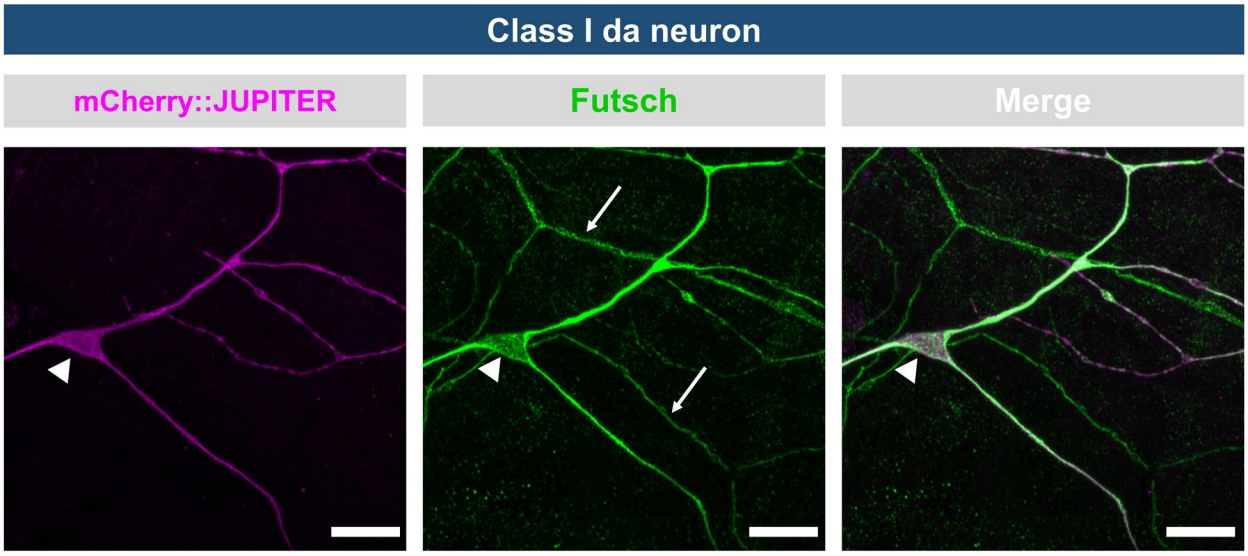

Figure S2. Class I da neuron microtubule labelling. Representative image of third instar larval Class I (ddaE) neuron labeled by class-specific GAL4[221] driven expression of UAS-mCherry::Jupiter to mark stable microtubules (magenta) (n=10 class I neurons). Larval filets were subjected to immunohistochemical labeling with antibodies against the microtubule binding protein Futsch (green), which labels all dendrites of all da neuron dendritic arbors (classes I-IV), and mCherry to mark the expression of the microtubule binding protein Jupiter (magenta). The location of the Class I ddaE cell body is denoted by the arrowhead in each panel, while the arrows mark dendrites emanating from other adjacent da neuron subtypes that are not labeled by the Class I driven Jupiter expression. The merge image clearly reveals overlap between these two microtubule binding proteins. Scale bar corresponds to 10 microns. Related to Figure 1.

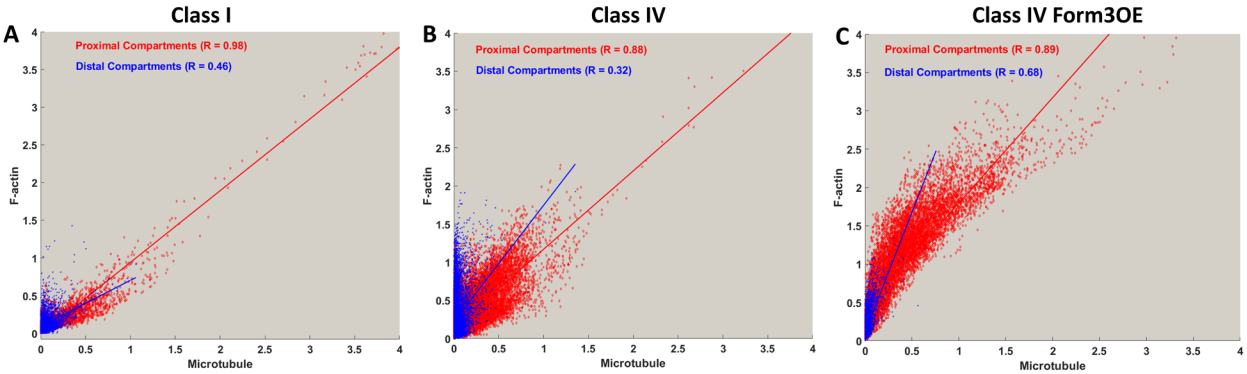

Figure S3. The distribution of F-actin as a function of microtubule in proximal (the closest 20% of the compartments, in Red) and distal (the farthest 20% of the compartments) dendritic compartments from Class I (A), Class IV WT (B) and Class IV Form3OE (C) neurons. Related to Figure 1 and 2. The correlation between microtubule and F-actin is lower for the distal compartments in all three neuron types, and lowest in Class IV WT.

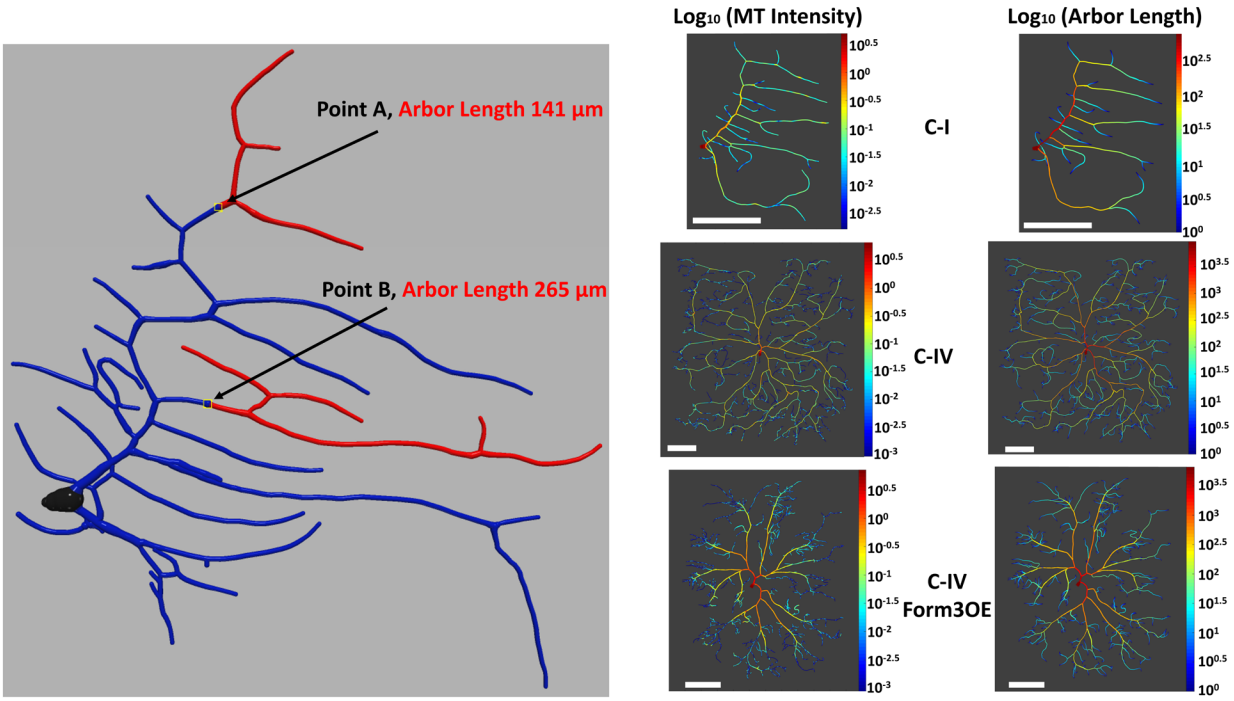

Figure S4. Dendritic arbor length and its association with local microtubule quantity. Arbor length of a compartment is defined as the total downstream length from that location. On the left figure, the red dendritic regions are the downstream arbors for the two representative compartments A and B. On the right, microtubule quantity and arbor length for Class I, Class IV and Class IV Form3OE neurons show similar centrifugal decrease. Related to Table 1.

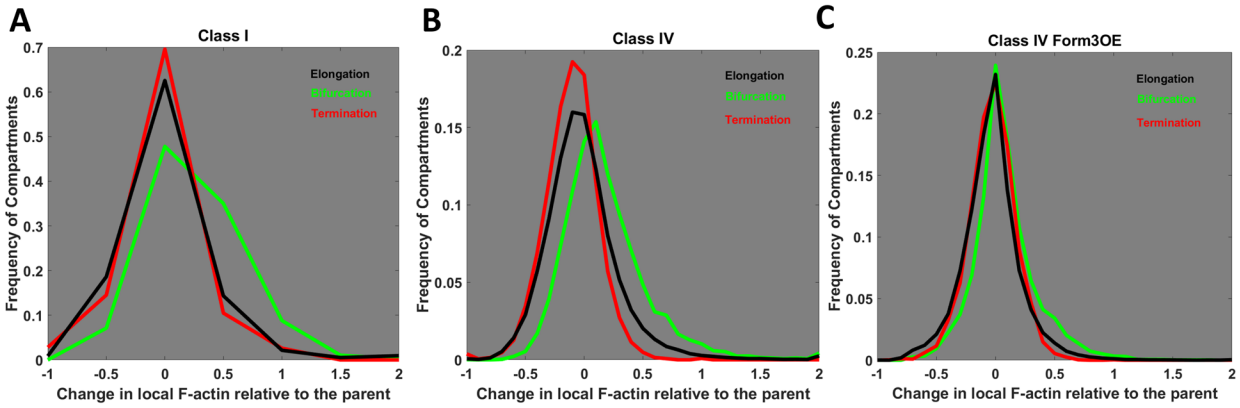

Figure S5. Frequency of the fold change in local F-actin concentration relative to the parent compartment for bifurcating (green), elongating (black) and terminating (red) compartments. Related to Figure 3. A value of 0 indicates unchanged F-actin concentration; a value of -1 indicates complete F-actin disappearance (100% decrease relative to parent compartment); and a value of +1 indicates doubling of F-actin concentration (100% increase relative to parent compartment). Class I (A), Class IV (B) and mutant Class IV Form3OE (C) distributions are shown separately.

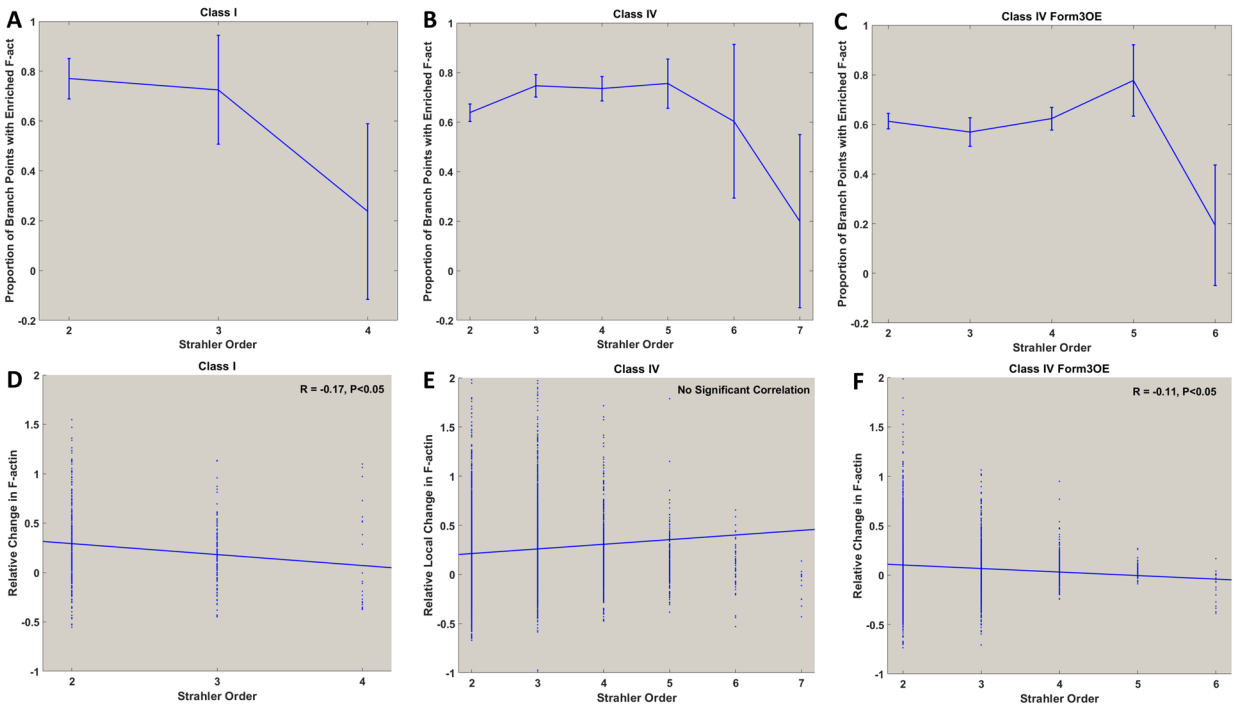

Figure S6. Strahler order based distribution of branch points and their local change in F-actin. Related to Figure 3. The top row (A, B, C) displays the proportion of branch points at each Strahler order with a positive local F-actin change for Class I (A), Class IV WT (B) and Class IV Form3OE (C) neurons. More than half the compartments from all Strahler orders (excluding the somatic regions i.e. the final Strahler order for each neuron type) from all three neuron types were F-actin enriched, i.e. an increase in local F-actin relative to the parent compartment. Error bars display standard deviation. The bottom row (D, E, F) displays the correlation between Strahler order and level of F-actin enrichment. Class I (D) and Class IV Form3OE (F) neurons show a negative correlation, indicating a reduction in F-actin enrichment levels while moving away from the terminals and towards the soma. Class IV neurons (E) show no correlation between Strahler order and F-actin enrichment level.

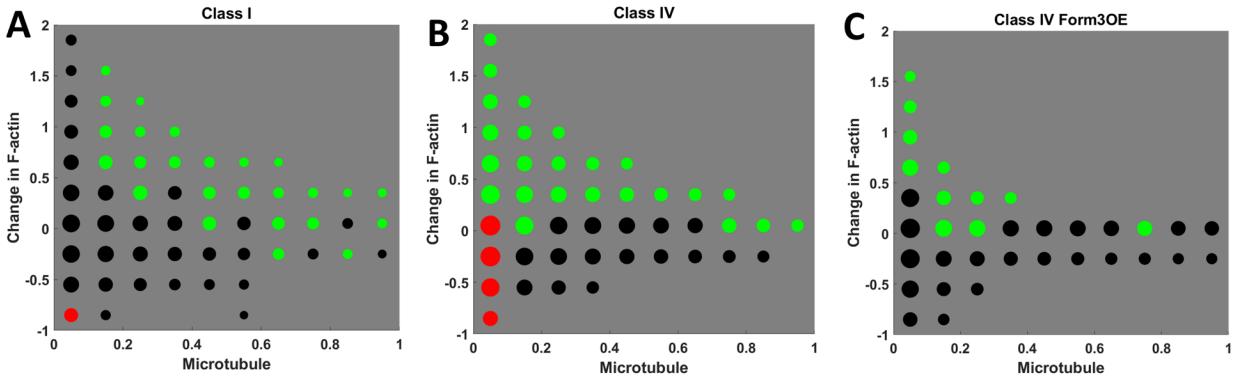

Figure S7. Two-dimensional distribution of all dendritic compartments based on local microtubule and local change in F-actin. Related to Table 1 and Figure 3. Class I (A), Class IV (B) and Class IV Form3OE (C) neurons are represented in the figure. The size of each circle is proportional to the log of the number of compartments with MT and F-act quantities in the corresponding range. Green and red circles represent high bifurcation and termination proportions (greater than 8%), respectively. The bifurcating and terminating regions have distinct cytoskeletal composition.

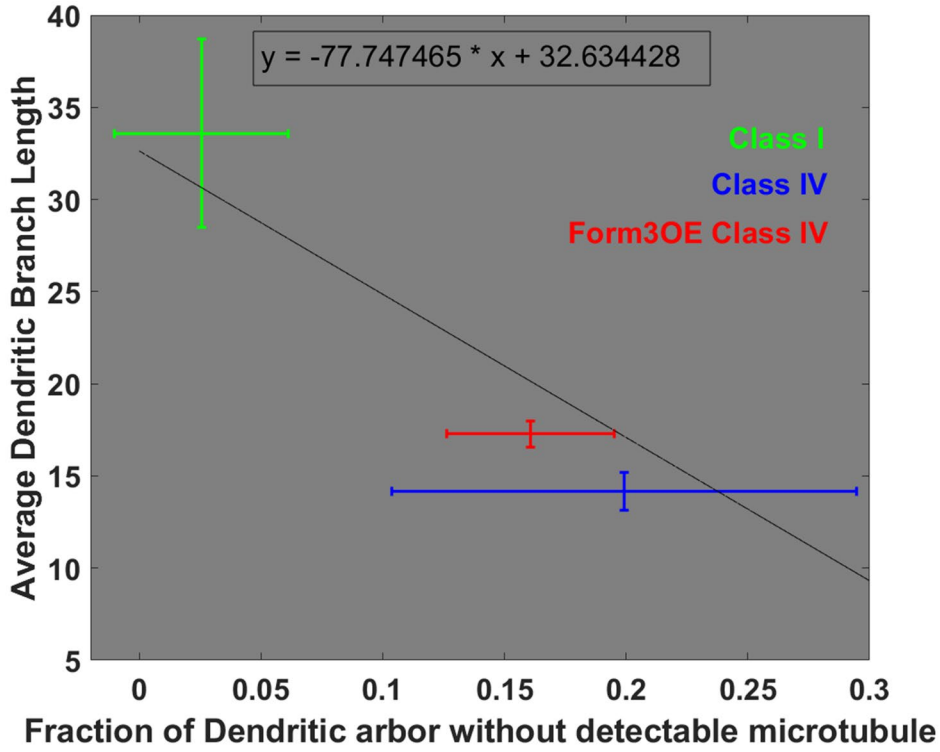

Figure S8. Negative correlation of mean branch length with the proportion of arbor lacking microtubule. Related to Table 1 and Figure 3. The vertical bars represent standard deviation of average branch length and the horizontal bars represent standard deviation of the fraction of arbor lacking microtubule.

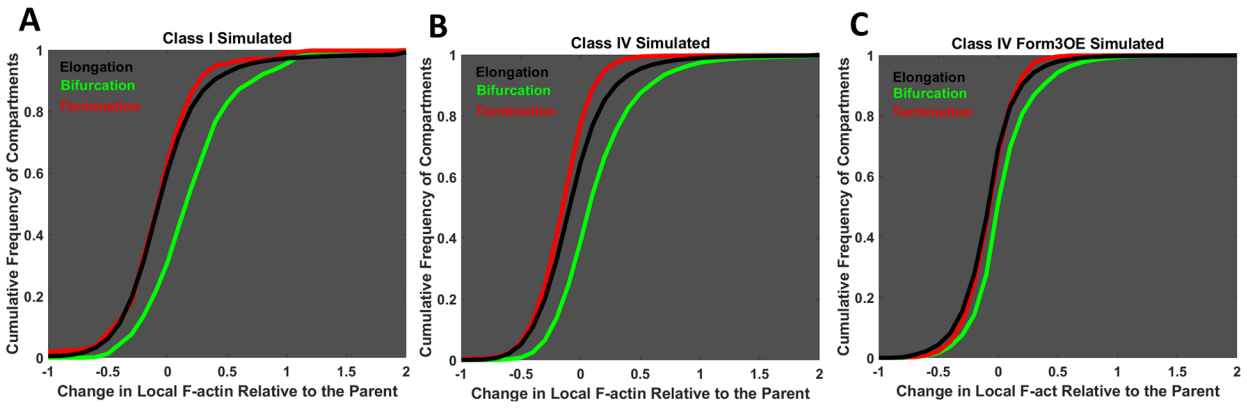

Figure S9. Analysis of the fold change in local F-actin concentration in simulated neurons. Related to Figure 3. Emergent cumulative frequency of the fold change in local F-actin concentration relative to the parent compartment for bifurcating (green), elongating (black) and terminating (red) compartments. Simulated Class I (A), Class IV (B) and mutant Class IV Form3OE (C) distributions are shown separately. In all three cases, the bifurcating probability distribution function is clearly separate from the terminating and elongating ones, well matching the corresponding experimental measurements.

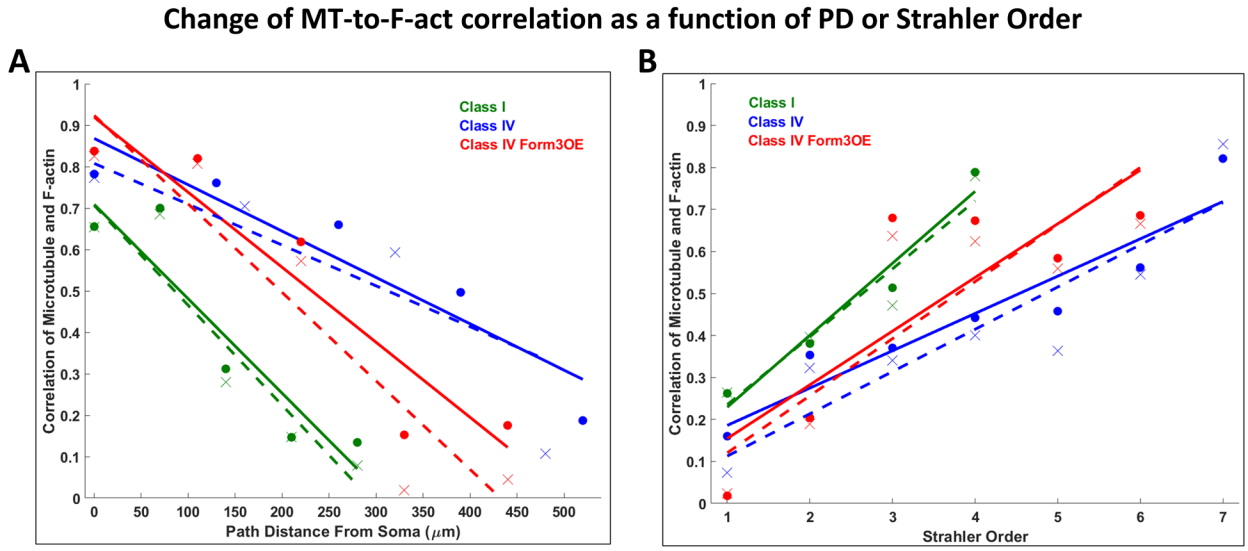

Figure S10. MT-to-F-act correlation in real and simulated neurons as functions of path distance and Strahler order. Related to Figure 2 and 6. Change of MT-to-F-act correlation as a function of path distance from soma (A), and Strahler order (B). Solid circles represent real neuron correlation distribution and 'x'-marks display the correlation distribution of the simulated neurons. Solid lines represent linear fits for the real neurons, dotted lines represent linear fits for the simulated neurons.

Supplemental Tables

Table S1. Comparison of MT-to-Fact and MT-to-Arbor Length correlation between real and simulated da neuron arbors. Related to Table 1, Figure 2, Figure 5 and Figure 6. Comparison between real (blue) and simulated (red) neurons of the correlation between microtubule and F-actin expression at different path distances from the soma and of the correlation between microtubule and arbor length in bifurcating and terminating branches.

Pearson Correlation Coefficients	Class I	Class IV	Class IV Form3OE
MT-F-act, Closest 20% compartments from the soma (Observed)	0.98	0.88	0.89
MT-F-act, Closest 20% compartments from the soma (Emergent)	0.98	0.87	0.89
MT-F-act, Farthest 20% compartments from the soma (Observed)	0.46	0.32	0.68
MT-F-act, Farthest 20% compartments from the soma (Emergent)	0.44	0.47	0.67
MT-Arbor Length bifurcating Branches (Observed)	0.65	0.77	0.87
MT-Arbor Length bifurcating Branches (Emergent)	0.65	0.76	0.86
MT-Arbor Length terminal Branches (Observed)	0.26	0.16	0.02
MT-Arbor Length terminal Branches (Emergent)	0.26	0.07	0.02

Table S2. Comparison of observed (real neurons) and emergent (simulated neurons) morphological properties. Related to Figure 2, Figure 5 and Figure 6.

Properties	*Class I*	*Class IV*	*Class IV Form3OE*
Total Length (µm) (Observed)	1680 ± 166	19305 ± 1510	12591 ± 985
Total Length (µm) (Emergent)	1653 ± 191	19033 ± 1416	12154 ± 1761
Total Tips (Observed)	26 ± 4.8	683 ± 44.7	365 ± 29.9
Total Tips (Emergent)	26 ± 5.2	673 ± 46.3	354 ± 51.5
Length Asymmetry (Observed)	0.559 ± 0.052	0.549 ± 0.017	0.570 ± 0.019
Length Asymmetry (Emergent)	0.559 ± 0.055	0.553 ± 0.018	0.568 ± 0.021
Topological Asymmetry (Observed)	0.607 ± 0.077	0.610 ± 0.024	0.598 ± 0.015
Topological Asymmetry (Emergent)	0.602 ± 0.089	0.608 ± 0.025	0.593 ± 0.019
Length Caulescence (Observed)	0.631 ± 0.107	0.450 ± 0.067	0.497 ± 0.063
Length Caulescence (Emergent)	0.616 ± 0.115	0.471 ± 0.061	0.472 ± 0.080
Topological Caulescence (Observed)	0.579 ± 0.091	0.470 ± 0.080	0.488 ± 0.053
Topological Caulescence (Emergent)	0.565 ± 0.101	0.469 ± 0.066	0.487 ± 0.033

Table S3. Average branch length and ratio between microtubule and F-actin quantities in real and simulated neurons as well as in bifurcating and terminating branches. Related to Figure 2, Figure 5 and Figure 6.

Neuron Type	C1	C4	C4 Form3OE	C1 Sim	C4 Sim	C4 Form3OE Sim
Branch Length (μm)	33.57 ± 5.11	14.17 ± 1	17.27 ± 0.7	33.45 ± 5.32	14.17 ± 1	17.21 ± 0.72
MT to F-act ratio	0.89 ± 0.32	0.38 ± 0.14	0.25 ± 0.04	0.89 ± 0.32	0.37 ± 0.14	0.26 ± 0.04
Branch Length (Bifurcating) (μm)	24.91 ± 4.01	15.35 ± 1.02	16.43 ± 1.22	24.75 ± 4.5	15.39 ± 1.07	16.5 ± 1.21
MT to F-act ratio (Bifurcating)	1.13 ± 0.27	0.55 ± 0.19	0.3 ± 0.04	1.13 ± 0.26	0.55 ± 0.19	0.30 ± 0.04
Branch Length (Terminating) (μm)	41.88 ± 8.07	12.98 ± 1.29	18.11 ± 0.75	41.78 ± 8.07	12.96 ± 1.32	17.95 ± 0.60
MT to F-act ratio (Terminating)	0.63 ± 0.39	0.07 ± 0.02	0.1 ± 0.02	0.63 ± 0.39	0.08 ± 0.02	0.1 ± 0.02

Table S4. Pearson correlation coefficients of arbor length against morphological and cytoskeletal parameters at the resolution of single (2 μm long) compartments for simulated neurons. Related to Table 1.

Cell Type	MT Quantity	F-act Quantity	MT + F-act Quantity	Path Distance from Soma	Branch Order
Class I	0.66	0.54	0.61	-0.47	-0.34
Class IV	0.76	0.42	0.61	-0.44	-0.41
Class IV Form3OE	0.87	0.76	0.82	-0.48	-0.39

Transparent Methods

Drosophila strains and live confocal imaging

Drosophila stocks were reared at 25˚C on standard cornmeal-molasses-agar media. Age-matched wandering third instar larvae of both sexes were used for all experiments. Fly strains used in this included: *w1118, UAS-GMA::GFP; GAL4[477],UAS-mCherry::Jupiter* (Das et al., 2017) (Class IV cytoskeletal reporter strain); *w1118, UAS-GMA::GFP;+;GAL4[221],UAS-mCherry::Jupiter* (Class I cytoskeletal reporter strain); *UAS-form3-B1* (Tanaka et al., 2004). *w1118* was used as a genetic background control for outcrosses to the multi-fluorescent cytoskeletal transgene reports. We previously confirmed that expression of the F-actin and microtubule transgene reporters did not themselves exert any effects on dendritic development (Das et al., 2017). Live confocal imaging of age-matched third instar larval mature da neuron Class I and Class IV arbors was performed as previously described (Das et al., 2017; Nanda et al., 2018a, 2018b). Briefly, larvae were immersed in a 1:5 (v/v) diethyl ether to halocarbon oil on a cover slipped glass slide and neurons expressing fluorescent protein cytoskeletal reporter transgenes were visualized on a Zeiss LSM 780 confocal microscope. Dissection and immunofluorescent labeling of third instar larval filets was performed as previously described (Sulkowski et al., 2011). Primary antibodies used in the study were rabbit anti-mCherry (used at 1:500) (Abcam; catalog # ab167453) and mouse anti-Futsch (22C10; used at 1:200) (Developmental Studies Hybridoma Bank; catalog # 22C10) (See Figure S2 for comparison of MT signal between UAS-mCherry::Jupiter and Futsch). Secondary antibodies were donkey anti-mouse Alexa fluor 488 (1:200) (Invitrogen; catalog # A21202) and donkey anti-rabbit Alexa fluor 555 (1:200) (Invitrogen; catalog # A-31572). Images were collected as z-stacks at a step size of 1-2 microns and 1024 x 1024 resolution using a 20X air objective (Plan Apo M27, NA 0.8) and 1 airy unit for the pinhole. A total of 19 Class I ddaE, 10 Class IV ddaC, 9 mutant Class IV ddaC Form3OE neurons were imaged, reconstructed, analyzed, and modeled. The digital morphological tracings and enhanced multi-signal ESWC files of all 38 neurons have been deposited to NeuroMorpho.Org (Ascoli et al., 2007) as part of the Ascoli and Cox archives. Images and the processed data have been deposited in Mendeley.com along with the analysis and modeling code (DOI: doi.org/10.17632/v3ncxmj6fn.1) for open access release upon publication of this manuscript.

Neuromorphometric analyses

Confocal images were semi-automatically reconstructed and edited in neuTube (Feng et al., 2015). Larval da neurons are relatively flat with limited dendritic arborization in the Z dimension. Therefore, images containing high levels of noise (usually the top and bottom of the Z stacks) were removed and maximum intensity projection of the remaining stacks were used to guide the reconstructions process. The MT signal from the red channel and F-act signal from the green channel were combined in FIJI (Schindelin et al., 2012) to create a third pseudo membrane channel from which the initial tracing was carried out. TREES Toolbox (Cuntz et al., 2010) was then used to resolve inaccuracies in tree topology and to resample the dendritic tree into compartment of uniform length (approximately 2 µm). These edited and resampled trees where then manually curated in neuTube once more and scaled from pixels to physical unit (µm) to generate the final SWC files. To test whether the morphologies imaged from the combined MT and F-act signal used in this study match with previous membrane tagged tracings, we downloaded legacy Class IV ddaC (N= 16) and Class I ddaE (N= 19) neural reconstructions from NeuroMorpho.Org (Nanda et al., 2018b; Sulkowski et al., 2011) and compared their overall size and complexity with the neurons from the current study. The total dendritic lengths were not statistically different ($P>0.05$, two-tailed t-test) in either Class IV (18,753±5704 µm from NeuroMorpho.Org vs. 19,305±1510 µm in the current study) or Class I neurons (1897±489 µm from NeuroMorpho.Org vs. 1680±166 µm in the current study).

Multi-signal ESWC reconstructions (Nanda et al., 2018a) were produced in Vaa3D, using the *Multichannel_Compute* plugin, with the reconstructed SWC files and the multichannel images as input and a threshold of 10 for both channels (i.e. any intensity below 10 out of 255 was considered as 0). Specifically, the plugin was run twice, first with the basic SWC as the reconstruction and MT (red) as the secondary channel; and then a second time with the resultant multi-signal SWC from the first run as the reconstruction and F-act (green) as the secondary channel. A combination of the red and green channels was used as the primary channel for both runs. The final multi-signal reconstructions contained sub-structural information for both MT and F-act. The two signals were then represented and analyzed as cytoskeletal quantity (MT or F-act quantity) in each compartment, which was calculated as a product of

three parameters: average signal intensity, fraction of compartment volume occupied by the signal and the compartment thickness. The minimum signal intensity of 10 in a 0 to 255 scale was used as a threshold to differentiate between noise and signal, and to find the proportion of voxels containing the signal within each compartment. The average intensity of the identified voxels was then normalized to a scale of 0 to 1, from the scale of 0 to 255, before being multiplied with compartment thickness. The local cytoskeletal quantity (**CQ**) (i.e. quantity if MT/F-act signal within a compartment) is thus defined as:

$$\mathbf{CQ} = \boldsymbol{F} * \boldsymbol{ASI} * \boldsymbol{W}$$

where **F** is the fraction of the compartment volume occupied by the signal, **ASI** is average signal intensity within that fraction volume, and **W** is local dendrite width, i.e. the diameter of the compartment.

Custom scripts were written leveraging the TREES Toolbox (Cuntz et al., 2010) functions to calculate and plot multiple topological and cytoskeletal properties both locally and as arbor-wide distributions, including analysis of dendritic length and cytoskeletal protein expression vs. path distance from soma and Strahler order. Cytoskeletal quantities were normalized based on average total MT and average total F-act of Class IV WT neurons. We analyzed a large number of dendritic compartments from all three neuron groups: 16,052 from Class I (15,079 elongations , 477 bifurcations and 496 terminations), 98,520 from Class IV WT (84,872 elongations, 6819 bifurcations, 6829 terminations), and 66,305 from Class IV Form3OE (59,738 elongations, 3279 bifurcations, 3288 terminations).

Mathematical definitions of asymmetry and caulescence

Topological asymmetry (Van Pelt et al., 1992) is defined as the average over all neuron bifurcations of the following function:

$$\boldsymbol{A_{td}} = \mathbf{0} \qquad \text{if} \qquad \boldsymbol{l_{td}} = \boldsymbol{r_{td}} = \mathbf{1}$$

$$\boldsymbol{A_{td}} = |\boldsymbol{l_{td}} - \boldsymbol{r_{td}}| \,/\, (\boldsymbol{l_{td}} + \boldsymbol{r_{td}} - \mathbf{2}) \qquad \text{otherwise,}$$

where $\boldsymbol{l_{td}}$ and $\boldsymbol{r_{td}}$ represent the numbers of terminal tips (or terminal degree) respectively in the left the right subtrees of the bifurcation.

Length asymmetry is similarly defined as the average over all neuron bifurcations of the following function:

$$\boldsymbol{A_l} = |\boldsymbol{l_l} - \boldsymbol{r_l}| \,/\, (\boldsymbol{l_l} + \boldsymbol{r_l})$$

where $\boldsymbol{l_l}$ and $\boldsymbol{r_l}$ represent the arbor length respectively of the left the right subtrees of the bifurcation.

Topological caulescence (Brown et al., 2008) is the weighted topological asymmetry across the dendritic path from the soma to the terminal with the highest centrifugal branch order:

$$\boldsymbol{C_{td}} = \sum |\boldsymbol{l_{td}} - \boldsymbol{r_{td}}| \;/\; \sum (\boldsymbol{l_{td}} + \boldsymbol{r_{td}})$$

Length caulescence is the weighted length asymmetry across the dendritic path from the soma to the terminal with the highest path distance from the soma:

$$\boldsymbol{C_l} = \sum |\boldsymbol{l_l} - \boldsymbol{r_l}| \;/\; \sum (\boldsymbol{l_l} + \boldsymbol{r_l})$$

Estimation of image resolution and its influence on dendritic diameter correlations

We calculated the theoretical resolution limit of the imaging system utilized in this study using the full width half maximum (FWHM) definition, whereas the lateral resolution in confocal laser scanning

microscopy is given by 0.51*lambda/NA, where lambda is the excitation wavelength and NA is the numerical aperture. In our case, NA = 0.8 and lambda = 488 (corresponding to GFP). Using these formula and parameters, we calculate a lateral resolution of 311.1 nm. Since the imaging system is unable to differentiate objects below this resolution, we use 311.1 nm as the maximum error value to estimate the theoretically greatest possible increase in linear correlation between diameter and arbor length. We treat the difference between the real (measured) and the expected (based on its downstream arbor length) diameter value as noise and proceed to reduce it by a correction factor sampled for each neuronal compartment from a uniform distribution bounded by the smaller of the resolution limit (311.1 nm) and the measured difference for that compartment. We run the simulation 10 times for each neuron type and calculate the average correlation across the 10 trials. While, as expected, correlation increases for all neuron groups, they remain less predictive than local microtubule except for Class I (see Results).

Relative change in F-actin

We first calculated the change in F-act quantity of every compartment from its parent compartment by simply subtracting the current quantity of F-act from that of the parent compartment. We then compute the ratio of F-act change to the parent F-act quantity to yield the relative F-act change (FΔ):

$$\boldsymbol{F\Delta} = \frac{(\boldsymbol{Fc} - \boldsymbol{Fp})}{\boldsymbol{Fp}}$$

where Fp and Fc are the F-actin quantities of the parent and of the current compartment, respectively.

Microtubule and F-actin based tree generation model

The data-driven model to simulate synthetic dendritic arbors was implemented in MATLAB (MathWorks, Natick, MA). This stochastic model uses three sampling grids: one for topological events and two for cytoskeletal composition (one each for elongating and bifurcating compartments). These grids can be thought of as two-dimensional matrices whose individual entries are populated with appropriate data extracted from real neurons (topological event in the first grid, cytoskeletal composition in the second and third) binned by the corresponding local microtubule and F-actin quantities.

The simulations started by sourcing the dendritic roots stemming from the soma of a real neuron as the 'active' compartments. Then, for every active compartment, the model identified the topological grid bin most closely matching the microtubule and F-actin quantities and sampled one of three topological events (elongation, bifurcation or termination) according to the following process. Data in the bin were first sorted by descending integral microtubule (***IM***), defined for the (i+1)th compartment as:

$$\boldsymbol{IM_{i+1}} = (\boldsymbol{IM_i} * \mathbf{0.99}) + (\boldsymbol{MQ_i} * \mathbf{0.01})$$

where ***MQ*** is the microtubule quantity and the ith compartment is the parent of the (i+1)th compartment. Integral microtubule can equivalently be expressed as:

$$\boldsymbol{IM_{i+1}} = \mathbf{0.99} * \boldsymbol{MQ_0} + \sum_{\boldsymbol{j=1}}^{\boldsymbol{i}} (\mathbf{0.99})^{\boldsymbol{i-j}} * \boldsymbol{MQ_j}$$

where $\boldsymbol{MQ_0}$ is the microtubule quantity at the root compartment. The integral microtubule quantifies the progression of microtubule across the dendritic path from the soma to the current location. For sampling within a bin of n elements, first a number m was randomly chosen between 1 and n. This was followed by choosing a number between 1 and m and the process was repeated four additional times (totaling six iterations). This procedure reduces the effect of noise in the real data and increases the probability of sampling data points with higher integral microtubule earlier during a simulation. Once an element was sampled, it was removed from the data bin. If an elongation was sampled, a new compartment was added, sampling its cytoskeletal composition from the elongation grid with the same process described above. In case of bifurcations, two new compartments were added sampling their cytoskeletal compositions from the bifurcation grid. In case of termination, the compartment 'inactivated', ending the branch. The simulations stopped when all compartments inactivated.

All analysis and modeling code have been deposited to Mendeley.com (DOI: http://dx.doi.org/10.17632/v3ncxmj6fn.1) for open access release upon publication of this manuscript.

Glossary

Arbor length: total downstream length of dendritic arbor from the given compartment. The arbor length of the soma is that neuron's total neurite length and the arbor length of any dendritic terminal tip is zero.

Branch thickness: diameter of the compartment (current point).

Compartment: cylindrical segment that starts at the parent point and ends at the current point of a digital reconstruction.

> **Active compartment:** compartment that has just been created in simulation, and its cytoskeletal composition is being determined, followed by its topological property, i.e. whether the compartment will elongate further, bifurcate or terminate.
>
> **Bifurcating compartment**: a compartment that branches out into two child compartments.
>
> **Child compartment**: the compartment immediately after the current compartment. The terminal compartments (tips) have no child.
>
> **Elongating compartment**: a compartment that elongates into one child compartments.
>
> **Parent compartment**: the compartment immediately before the current compartment in the direction towards the soma. All dendritic compartments have one parent compartment. However, a parent compartment may have one to two child compartments. Only terminal compartments (that do not have child compartments) are not parent compartments themselves, and only the root node of a tree has no parent compartment.
>
> **Terminating compartment**: a compartment that terminates (branch tip), hence has no child compartments.

Data Grid: a two-dimensional matrix whose dimensions are local microtubule and local F-actin quantities. Each matrix entry corresponds to a small range (bin) of microtubule and F-actin values. The topological event probability grid contains in each entry the occurrences of extensions, bifurcations, and continuations that where observed at the corresponding ranges of MT and F-act quantities. The cytoskeletal (elongation and bifurcation) grids contain in each entry the MT and F-act quantities of the child compartment(s).

Descending Integral microtubule: defined for $(i+1)^{th}$ compartment as

$$\boldsymbol{IM_{i+1} = (IM_i * 0.99) + (MQ_i * 0.01)}$$

where ***MQ*** is the microtubule quantity and the i^{th} compartment is the parent of the $(i+1)^{th}$ compartment. Integral microtubule can equivalently be expressed as:

$$\boldsymbol{IM_{i+1} = 0.99 * MQ_0 + \sum_{j=1}^{i} (0.99)^{i-j} * MQ_j}$$

where $\boldsymbol{MQ_0}$ is the microtubule quantity at the root compartment.

Path distance: distance (in μm) of a dendritic location from the soma.

Strahler order: a centripetal branch numbering system, where all terminal branches are assigned the Strahler order of 1; if a non-terminal branch has children of unequal Strahler orders, its Strahler order is

set as the highest of those values; if a non-terminal branch has children of equal Strahler order n, its Strahler branch order is n+1. Thus, Strahler order of 2 is assigned to non-terminal branches that would become terminals if all the current terminal branches (with Strahler order of 1) were removed. The Strahler order therefore starts at the terminal and progressively increases until reaching the soma.

Topological event: occurrence of branch elongation, bifurcation or termination.

Supplemental References

Ascoli, G.A., Donohue, D.E., Halavi, M., 2007. NeuroMorpho.Org: A central resource for neuronal morphologies. J. Neurosci. 27, 9247–9251.

Cuntz, H., Forstner, F., Borst, A., Häusser, M., 2010. One rule to grow them all: A general theory of neuronal branching and its practical application. PLoS Comput. Biol. 6, e1000877.

Das, R., Bhattacharjee, S., Patel, A.A., Harris, J.M., Bhattacharya, S., Letcher, J.M., Clark, S.G., Nanda, S., Iyer, E.P.R., Ascoli, G.A., Cox, D.N., 2017. Dendritic cytoskeletal architecture is modulated by combinatorial transcriptional regulation in Drosophila melanogaster. Genetics 207, 1401–1421.

Feng, L., Zhao, T., Kim, J., 2015. neuTube 1.0: A new design for efficient neuron reconstruction software based on the SWC Format. eNeuro 2, ENEURO.0049-14.2014.

Nanda, S., Chen, H., Das, R., Bhattacharjee, S., Cuntz, H., Torben-Nielsen, B., Peng, H., Cox, D.N., Schutter, E. De, Ascoli, G.A., 2018a. Design and implementation of multi-signal and time-varying neural reconstructions. Sci. Data 5, 170207.

Nanda, S., Das, R., Bhattacharjee, S., Cox, D.N., Ascoli, G.A., 2018b. Morphological determinants of dendritic arborization neurons in Drosophila larva. Brain Struct. Funct. 223, 1107–1120.

Schindelin, J., Arganda-Carreras, I., Frise, E., Kaynig, V., Longair, M., Pietzsch, S., Rueden, C., Saalfeld, S., Schmid, B., Tinevez, J.Y., Pietzsch, T., Preibisch, S., Rueden, C., Saalfeld, S., Schmid, B., Tinevez, J.Y., White, D.J., Hartenstein, V., Eliceiri, K., Tomancak, P., Cardona, A., 2012. Fiji: an open-source platform for biological-image analysis. Nat Methods 9, 676–682.

Sulkowski, M.J., Iyer, S.C., Kurosawa, M.S., Iyer, E.P.R., Cox, D.N., 2011. Turtle functions downstream of Cut in differentially regulating class specific dendrite morphogenesis in Drosophila. PLoS One 6, e22611.

Tanaka, H., Takasu, E., Aigaki, T., Kato, K., Hayashi, S., Nose, A., 2004. Formin3 is required for assembly of the F-actin structure that mediates tracheal fusion in Drosophila. Dev. Biol. 274, 413–425.

Van Pelt, J., Uylings, H.B.M., Verwer, R.W.H., Pentney, R.J., Woldenberg, M.J., 1992. Tree asymmetry-A sensitive and practical measure for binary topological trees. Bull. Math. Biol. 54, 759–784.